ELSEVIER

Dyes and Pigments, Vol. 30, No. 3, pp. 183–200, 1996

0143-7208/96 $15.00 + 0.00

0143-7208(95)00076-3

The Solid State Structure of CI Disperse Orange 44

J. F. Malone

School of Chemistry, The Queens University of Belfast, Belfast BT9 5AG, UK

S. J. Andrews

ICI Chemicals and Polymers, The Heath, Runcorn, Cheshire, WA7 4QE, UK

J. F. Bullock & R. Docherty*

Zeneca Specialties Research Centre, Hexagon House, Blackley, Manchester M9 3ZS, UK

(Received 20 July 1995; accepted 22 August 1995)

ABSTRACT

The crystal structure of CI Disperse Orange 44 has been solved using direct methods and refined by least squares to R = *0·095. The structure consists of planar azobenzene molecules stacked in columns up the* b*-axis. The asymmetric unit consists of two molecules which differ in the conformation of the terminal* $-CH_2CH_2CN$ *groups. The molecular structures and solid state packing arrangements are compared with previously published data. Crystal packing calculations and high resolution powder diffraction studies have been employed to examine the likely structure of a mixed crystal with CI Disperse Orange 44 as the 'host' and CI Disperse Red 54 as an 'incorporated impurity'.*

1 INTRODUCTION

The relationship between molecular structure, solid state packing arrangements and dye/pigment performance characteristics has over recent years become an area of increasing investigation.[1–5] Properties such as solubility and saturation value within the fibre are related to the free energy of the dye molecule in the crystalline state.[6] Vapour pressures and heats of sublimation

*Corresponding author.

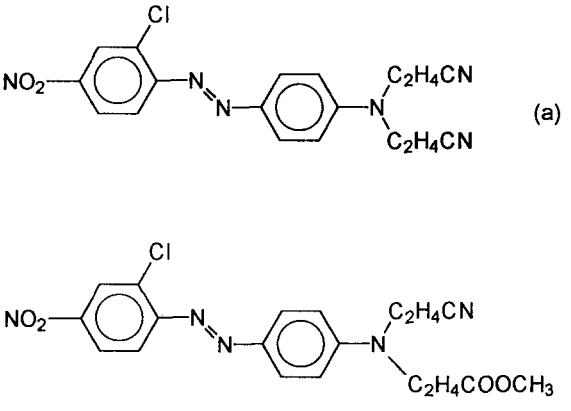

Fig. 1. The molecular structure of (a) CI Disperse Orange 44 and (b) CI Disperse Red 54.

have been determined by a number of authors in order to relate intermolecular interactions to properties and performance features in various dyeing and printing application processes.[7–9]

As in a previous paper[10] single crystal X-ray diffraction studies and crystal packing examinations have been employed to determine both the structure and the important intermolecular interactions in the solid state of donor–acceptor azobenzene. In this work the structure of CI Disperse Orange 44 (Fig. 1a) has been solved using crystallographic direct methods. Crystal packing calculations have been employed to examine the important intermolecular interactions. Real, commercial dye molecules are rarely pure and often impurities of similar structure to the 'host' molecule become incorporated to form mixed crystals. In combination with high resolution X-ray powder diffraction, crystal packing calculations were used to quantify the effect of an included impurity dye molecule (CI Disperse Red 54, see Fig. 1b) on the packing of the host molecules.

2 EXPERIMENTAL

2.1 Crystal growth

Crystals of CI Disperse Orange 44 were grown from acetone solution and 0·2 g was dissolved in 30 ml hot acetone. The solution was screened to remove undissolved matter and then reheated to dissolve any dye which might have precipitated on cooling. The solution was then allowed to cool slowly overnight in an oil bath. The crystals formed were elongated although not true needle in form, being quite thick. A dark red crystal of dimensions

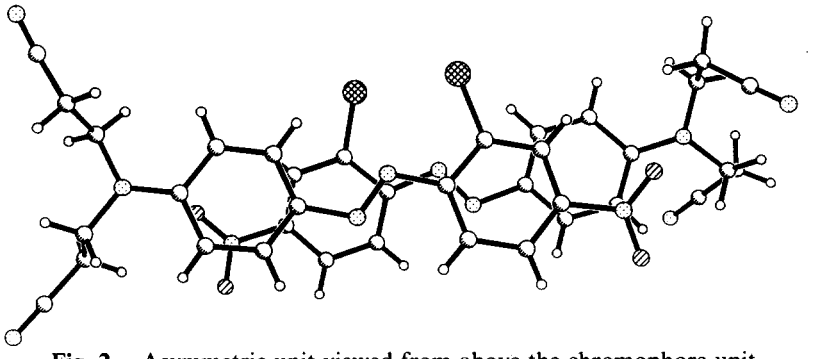

Fig. 2. Asymmetric unit viewed from above the chromophore unit.

0·2 × 0·3 × 1·25 mm was selected as being of suitable quality for single crystal X-ray analysis.

2.2 Structure solution

The crystal was mounted on a Siemens P3/V2000 diffractometer and irradiated using MoK_α radiation (graphite monochromated, λ = 0·7107 Å). The unit cell parameters were determined from 38 centered reflections with $7 < 2\theta < 26°$. Intensity data were collected at room temperature over a 2θ range between 3 and 60°. Of the 10771 observations collected (h:0->28; k: 0-> 18; 1: –19->19), 3979 reflections were flagged as observed based on the criteria $I>2\sigma(I)$.

The structure was solved using the direct methods options in SHELXS86[11] and refined by least squares on $|F^2|$ (SHELXL93[12]). All hydrogen atoms were located in a difference Fourier synthesis, but were included at calculated positions with common isotropic temperature factors for both methylene and benzene type carbons. The final R-factor obtained was 0·095; crystallographic data are given in Table 1. The asymmetric unit, which consists of two independent molecules, is shown viewed from above the chromophore in Fig. 2 and from the side of the chromophore in Fig. 3.

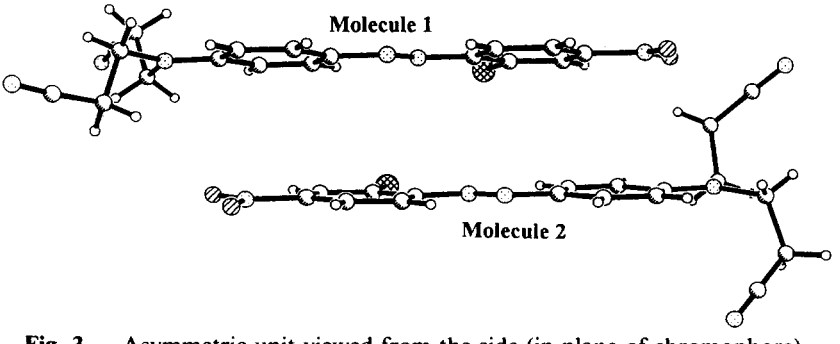

Fig. 3. Asymmetric unit viewed from the side (in plane of chromophore).

TABLE 1
Crystal Data for CI Disperse Orange 44

Formula	$C_{18}H_{15}N_6O_2Cl$
Molecular weight	382·8
Crystal system	Monoclinic
Space group	$P2_1/c$
Cell dimensions	a = 19·879(20) Å
	b = 13·428(11) Å
	c = 13·824(25) Å
	β = 90·88(12) °
Z	8
Volume	3693·1 Å^3
Density	1·38 Mg m^{-3}
Crystal form	Dark red blocks
Crystal dimensions	0·2 × 0·3 × 1·25 mm
μ	2·33 cm^{-1}
$F(000)$	1584
Diffractometer	Siemens P3/V2000
Radiation	MoK_α (graphite monochromated)
Wavelength	0·71073 Å
Temperature	295 K
Unique data measured	10771
Observed data	3937
Data in final refinement	2656
Data range	$3<2\Theta<60°$
	h: 0 → 28
	k: 0 → 18
	l: −19 → 19
R	0·099
R_w	0·096
Parameters refined	490
Data/parameter ratio	5·4
GoF	1·54

The unit cell is shown in Fig. 4 and the atomic co-ordinates for the asymmetric unit are given in Table 2.

2.3 Powder diffraction

X-Ray powder diffraction patterns are a fingerprint of the solid state arrangement adopted by a collection of molecules. In this paper, powder diffraction

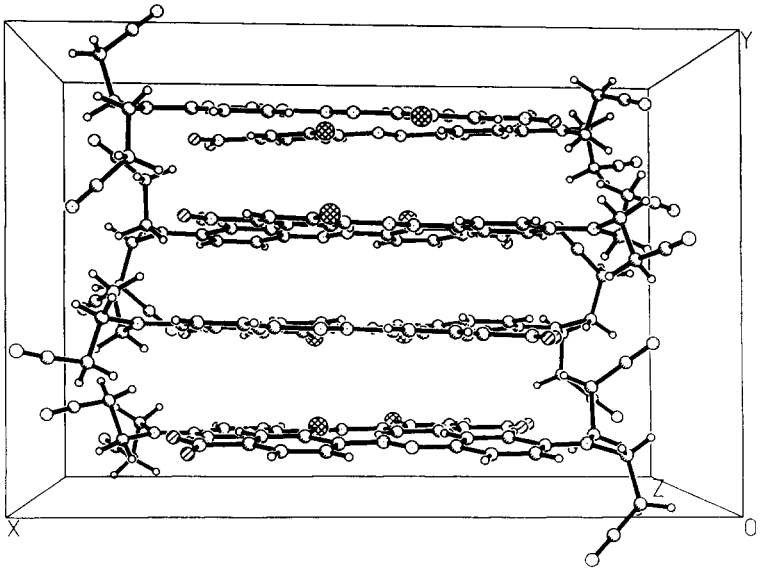

Fig. 4. The unit cell.

patterns are reported for CI Disperse Orange 44, collected on both a standard laboratory diffractometer and a high resolution instrument using a synchrotron radiation source. In Fig. 5, the X-ray diffraction traces for pure CI Disperse Orange 44 (a), the mixed crystal (b) and pure CI Disperse Red 54 (c) are shown. These data were collected on a Siemens D500 diffractometer using CuK_α radiation (λ = 1·541 Å). Sample (b) was produced as a mixed crystal containing 10% of CI Disperse Red 54 as an impurity by a standard diazotisation/coupling reaction using mixed coupling components.

Some of the powder diffraction studies reported in this paper were collected on the Synchrotron Radiation Source (SRS) at Daresbury Laboratory. The SRS is a 2 GeV electron storage ring, 96 m in circumference dedicated to the production of synchrotron radiation in a continuous spectrum from X-rays to infrared.

With a vertical divergence of typically 0·4 mrad and a continuum intensity of 10^4–10^6 times greater than that of a conventional laboratory source, the SRS yields powder diffraction patterns with better resolved reflections than may be achieved with conventional laboratory equipment

The superior resolution available is ideally suited to the study of low symmetry systems such as molecular materials, as these systems can produce extensive peak overlap in the diffraction pattern. The advantage of the SRS is that such peak overlap can be minimised, and thus the indexing of the pattern is far easier and less ambiguous. It is now possible to solve crystal structures of molecular materials from such high resolution patterns.[13,14]

TABLE 2
The Atomic Co-ordinates for CI Disperse Orange 44

Atom	*Label*	*x*	*y*	*z*	*Atom*	*Label*	*x*	*y*	*z*
1	C1	0·56019	0·86692	0·85553	43	C43	0·42310	0·64714	0·86174
2	C2	0·58406	0·87164	0·97614	44	C44	0·40218	0·63258	0·98171
3	C3	0·65136	0·86753	0·99976	45	C45	0·33463	0·63338	1·00491
4	H4	0·68874	0·86396	0·94403	46	H46	0·29636	0·64288	0·94943
5	C5	0·66957	0·86875	1·09603	47	C47	0·31860	0·62217	1·09919
6	N6	0·74179	0·86523	1·11948	48	N48	0·24509	0·62127	1·12710
7	O7	0·75837	0·86179	1·20499	49	O49	0·23071	0·60632	1·20877
8	O8	0·78174	0·86179	1·05498	50	O50	0·20515	0·63442	1·06206
9	C9	0·62392	0·87360	1·16944	51	C51	0·36564	0·61048	1·17406
10	H10	0·64054	0·87471	1·24418	52	H52	0·35073	0·60127	1·24832
11	C11	0·55622	0·87676	1·14528	53	C53	0·43317	0·60986	1·14859
12	H12	0·51931	0·88063	1·20163	54	H54	0·47147	0·60041	1·20404
13	C13	0·53492	0·87515	1·04825	55	C55	0·45079	0·62048	1·05366
14	N14	0·46689	0·87849	1·01740	56	N56	0·52078	0·62134	1·02165
15	N15	0·42638	0·87968	1·08876	57	N57	0·56155	0·61383	1·09255
16	C16	0·35695	0·88252	1·05973	58	C58	0·63031	0·61439	1·06393
17	C17	0·31176	0·89008	1·13345	59	C59	0·67795	0·60181	1·13698
18	H18	0·33007	0·89329	1·20733	60	H60	0·66141	0·59198	1·21041
19	C19	0·24354	0·89254	1·11575	61	C61	0·74691	0·60265	1·11593
20	H20	0·20934	0·89890	1·17536	62	H62	0·78356	0·59181	1·17341
21	C21	0·21729	0·88793	1·01967	63	C63	0·76841	0·61561	1·02201
22	C22	0·26565	0·88129	0·94469	64	C64	0·71780	0·62873	0·94687
23	H23	0·24810	0·87804	0·87044	65	H65	0·73346	0·63893	0·87307
24	C24	0·33315	0·88034	0·96519	66	C66	0·65124	0·62677	0·96964
25	H25	0·36835	0·87613	0·90662	67	H67	0·61420	0·63563	0·91237
26	N26	0·14954	0·88857	1 00076	68	N68	0·83650	0·61753	0·99870
27	C27	0·10088	0·90168	1·07760	69	C69	0·88980	0·59623	1·07044
28	H28	0·12277	0·94927	1·13262	70	H70	0·93386	0·63921	1·05299
29	H29	0·05598	0·93618	1·04824	71	H71	0 87236	0·61760	1·14107
30	C30	0·08284	0·80194	1·12448	72	C72	0·90971	0·48589	1·07355
31	H31	0·12705	0·76983	1·15836	73	H73	0·95827	0·47919	1·10896
32	H32	0·06417	0·75248	1·06863	74	H74	0·91301	0·45973	0·99990
33	C33	0·02983	0·81433	1·19740	75	C75	0·86256	0·42135	1·12362
34	N34	–0·01006	0·82941	1·25225	76	N76	0·82569	0·37057	1·16355
35	C35	0·12135	0·86723	0·90441	77	C77	0·85734	0·63193	0·89997
36	H36	0·15753	0·82580	0·86311	78	H78	0·90782	0·60345	0·89329
37	H37	0·07615	0·82355	0·91185	79	H79	0·82388	0·59113	0·85217
38	C38	0·10408	0·96428	0·85052	80	C80	0·85707	0·74240	0·86923
39	H39	0·14988	1·00495	0·83746	81	H81	0·80800	0·77278	0·88378
40	H40	0·07135	1·00867	0·89478	82	H82	0·86654	0·74687	0·79264
41	C41	0·07015	0·94184	0·75742	83	C83	0·90673	0·80204	0·92096
42	N42	0·04520	0·92269	0·68600	84	N84	0·94577	0·84834	0·96016

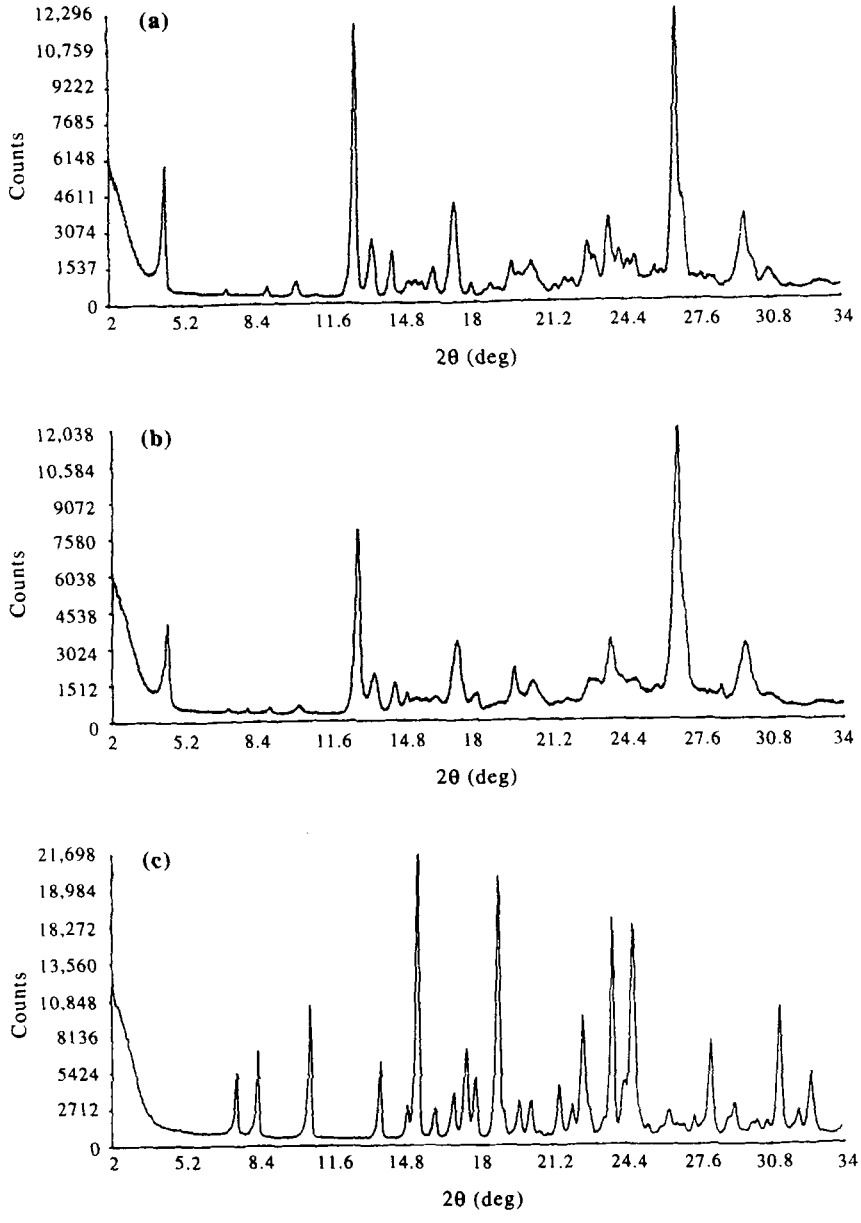

Fig. 5. The powder diffraction patterns collected on a standard laboratory instrument: (a) pure CI Disperse Orange 44; (b) the mixed crystal state; (c) pure CI Disperse Red 54.

High resolution powder diffraction data were collected using a θ–2θ scattering geometry on beamline 9·1 at the SRS. The wavelength and zeropoint correction were calibrated with NBS silicon to be 1·49841 Å and –0·0008°

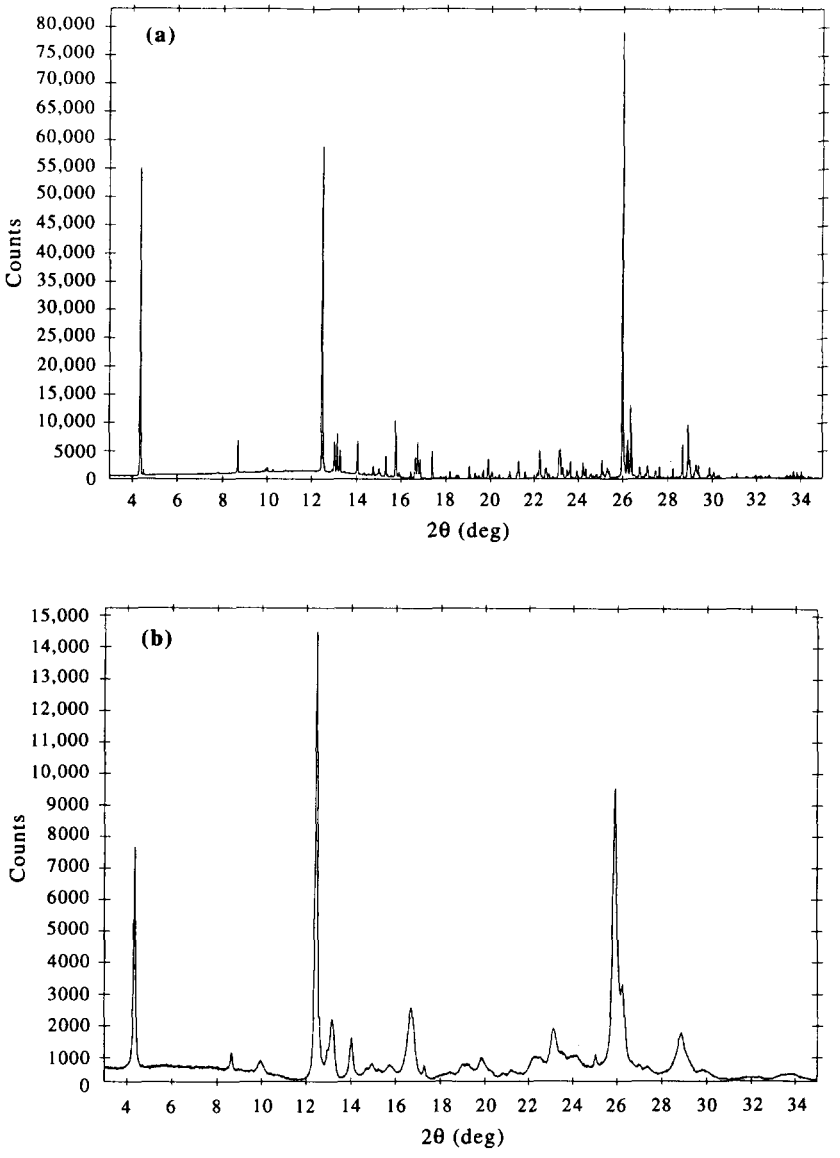

Fig. 6. The high resolution patterns for: (a) pure CI Disperse Orange 44; (b) the mixed crystal state.

2θ, respectively. Data for both the pure CI Disperse Orange 44 and the mixed crystal system were collected between 3 and 35° 2θ with a step size of 10 mdeg with a counting time of four seconds per step. The powder diffraction trace for pure CI Disperse Orange 44 is shown in Fig. 6a and that for the mixed crystal system is shown in Fig. 6b.

3 RESULTS AND DISCUSSION

3.1 Molecular structure

The crystal structure shows the unusual feature of two molecules in the asymmetric unit. This feature was also observed in the recent study on CI Disperse Red 167 reported within this journal.[15] The asymmetric unit is shown in Figs 2 and 3. Figure 2 shows the unit viewed from above the plane of the chromophore (i.e. down the *b*-axis). The upper molecule (molecule 1) is roughly 3·36 Å closer to the viewer, while the lower molecule (molecule 2) is related to molecule 1 by an approximate two-fold rotation axis, as shown on Fig. 3.

In Fig. 3 the asymmetric unit is viewed along the edge of the chromophores and shows the 3·3 Å intermolecular separation. This view shows the major difference in the molecules. The terminal $-CH_2CH_2CN$ are in different conformations. In molecule 1, the NCCC torsion angles are close to 180° (*anti* conformation), while in molecule 2 they are –77 and +66° (*gauche* conformation).

Since the two molecules in the asymmetric unit are not related by crystallographic symmetry, and are consequently refined separately, differences in bond distances and angles might be expected. In Table 3 the important molecular features for the two molecules in the asymmetric unit are compared with the range of reported values for donor–acceptor azobenzenes in the literature.[10,16]

In general there is good agreement between the molecular features of the new structure and previously reported data on donor–acceptor azobenzenes.

TABLE 3
The Important Structural Features in CI Disperse Orange 44 and Other Azobenzenes

Structural feature	*Molecule 1*	*Molecule 2*	*Range reported*[16]
N=N	1·267	1·284	1·254–1·294 (Å)
C–N(C_2)	1·369	1·398	1·353–1·415 (Å)
C–NO_2	1·469	1·518	1·446–1·472 (Å)
NNC[a]	112·2	112·9	113·0–118·9 (°)
NNC[b]	113·5	111·4	111·9–114·5 (°)
NNCC[b]	–2·3	–1·7	–1·3–6·0 (°)
NNCC[b]	2·4	3·1	–4·2–5·6 (°)
CCNC[c]	6·1	9·6	8·5–12·8 (°)
CCNC[c]	4·7	0·4	4·8–9·3 (°)

[a]Carbon(s) of the donor ring.
[b]Carbons of the acceptor ring with a *cis* conformation for the torsion angles.
[c]Carbons of the N–(C_2) group relative to the aromatic ring.

The N=N group is on the longer side of the range, which is probably due to the presence of the bulky chlorine substituent. The bond and torsion angles all show excellent agreement with the known data. The low values of the torsion angles are indications of the planarity of the molecule (except for the CH_2CH_2CN substituents). This is clear from Fig. 3. Although care must be taken in comparing bond distances for a structure with an *R*-factor near 10%, one interesting feature is the C–NO_2 bond distance of 1·518 Å. This is outside the known range for azobenzenes and longer than the published limit of 1·48 Å taken from a compendium of diffraction results.[17]

3.2 Crystal packing and intermolecular interactions

The molecules of CI Disperse Orange 44 arrange themselves in a monoclinic unit cell of dimensions a = 19·897, b = 13·428, c = 13·824 Å with β = 90·88°. The space group is $P2_1/c$, the most common space group for organic materials. With two molecules in the asymmetric unit and four asymmetric units defined by the space group symmetry there are eight molecules within the unit cell. This cell is shown in Fig. 4.

The entire structure consists of stacked molecules, with the mean planes through the molecules roughly parallel. The two independent molecules are about 3·3 Å apart and the symmetry related molecules are about 3·4 Å apart. Essentially, the solid state packing consists of columns running up the *b*-axis of the crystal structure with alternating asymmetric units related by symmetry. The molecules within the asymmetric unit are easily identified as those with chlorine molecules on the same side. The symmetry related molecules are those with chlorines on opposite sides. This is shown in Fig. 7.

This column arrangement is also found in a number of other donor–acceptor azobenzenes.[10] The most important interactions within these columns are the π–π interactions up this *b*-axis. Calculations on this and other azobenzene systems suggest these are the most important interactions

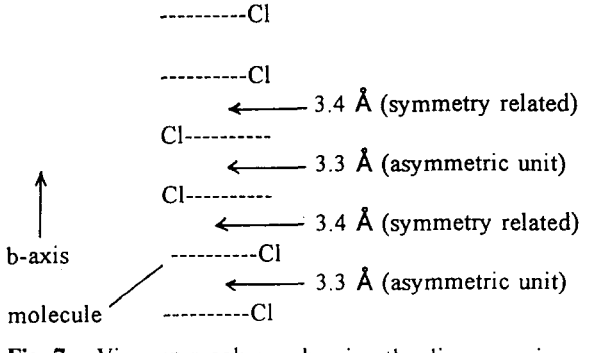

Fig. 7. View up a column showing the dimer spacings.

within this class of compounds. Each π–π interaction is worth about –8·0 kcal mol^{-1}, and so accounts for about 50% of the total lattice energy in the solid state (see following section). The π–π interactions are the result of a large number of relatively weak atom–atom interactions. On inspection of the dimer arrangement within the columns, some interactions look stronger than others, and the O=N:::::NC_2 non bonded contacts of 3·54 and 3·68 Å are very characteristic of the head-to-tail dimer arrangement found in other azobenzenes, where these contacts range from 3·42 to 4·10 Å. This head-to-tail arrangement is shown in Fig. 3.

The most important interactions along the *c*-axis appear to involve the chlorine in one molecule within one column and the aromatic hydrogens in a molecule in the next column. These Cl:::::H–Car contacts have been shown to play an important role in determining structural arrangements in halogenated systems.[18,19]

Electrostatic interactions seem to be the important interactions holding the molecules in one unit cell to molecules in the adjacent unit cell along the *a*-axis. Short contacts between the cyano groups of 3·22 and 3·29 Å seem to form a network within the (100) plane. Supplementary interactions seem to exist between these cyano groups and the nitro groups of adjacent molecules. This is illustrated in Fig. 8.

In summary, π–π interactions dominate along the *b*-axis holding the molecules in columns. These columns are held together in the *c*-direction thanks to Cl::::::H contacts and through a network of electrostatic interactions between the cyano groups in the *a*-direction.

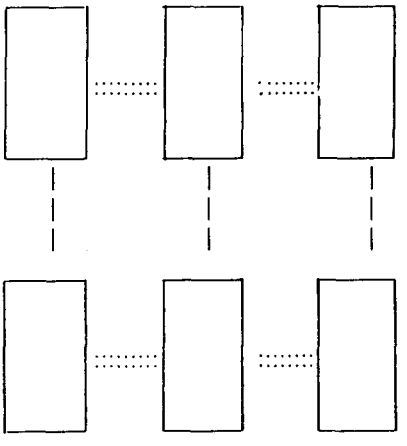

:::::: = Chlorine/hydrogen non-bonded contact
- - - = Cyano/cyano group interaction

Fig. 8. View down the *b*-axis showing the interactions holding the columns together in the *ac*-plane.

3.2.1 Crystal packing calculations

Crystal packing calculations were carried out using PCK83[20] and CERIUS.[21] In PCK83 the potentials were the default values with the additional chlorine potentials from Bernstein.[22] Charges were calculated using MOPAC.[23] In CERIUS the open force field parameters were used and the charges obtained from the charge equilibration method.[24] In both calculations the summation limit was set to 30 Å and no minimisation of the structure was allowed. The presence of two independent molecules in the asymmetric unit resulted in the calculation being performed centered on both molecules and the results averaged. The calculated lattice energies are compared against an experimental value determined from the sublimation enthalpy. The sublimation enthalpy was determined by measuring the vapour pressure of CI Disperse Orange 44 at a series of temperatures and using the Clausius–Clapeyron equation to provide the heat of sublimation. The vapour pressures were determined using a weight-loss effusion apparatus specifically designed for measuring low vapour pressures. The results are given in Table 4.

Good agreement exists between the calculated and experimental values for the lattice energy indicating a reasonable description of the important intermolecular interactions present within the system.

3.3 Mixed crystal structure

3.3.1 Qualitative picture

No peaks characteristic of the pure CI Disperse Red 54 solid state arrangement (Fig. 5c) are found in the mixed crystal pattern (Fig. 5b), indicating that the guest impurity has been incorporated into the CI Disperse Orange 44 lattice with only minor structural changes. The similarity between Figs 5a and b, showing the same major peaks occurring in similar positions, confirms the likely formation of a mixed crystal within the framework of the CI Disperse Orange 44 lattice.

Although it appears that no changes in the unit cell dimensions occur on incorporation (to be confirmed in the next section), the melting point of the

TABLE 4
Calculated and 'Experimental' Lattice Energies for CI Disperse Orange 44

Study	*Lattice energy (kcal mol^{-1})*
PCK83	−31·7
CERIUS	−32·3
Experiment	−33·9

TABLE 5
Melting Points and Heats of Fusion of Pure and Doped CI Disperse Orange 44

System	*Melting point (°C)*	*Heat of fusion ($J\,g^{-1}$)*
CI Disperse Orange 44 (pure)	197	115·9
2·5% CI Disperse Red 54	195	
5% CI Disperse Red 54	193	
7·5% CI Disperse Red 54	189	
10% CI Disperse Red 54	184	93·3

system and heat of fusion are reduced on the incorporation of the dopant, as is shown in Table 5. These reductions highlight the disruptive effect of dopant on the important intermolecular interactions within the host crystal structure.

A rough parameter used in crystal engineering for deciding whether a guest molecule can be included within a host structural lattice is the co-efficient of geometrical similarity (ϵ) which was first used by Kitaigordskii.[25] This geometrical parameter can be calculated by comparing the molecular volumes of host and guest as shown below

$$\epsilon = 1-|R-r|/R,$$

where R is the volume of the host molecule, r is the volume of the guest molecule and $|R-r|$ is the non-overlapping volume.

In the literature it has been proposed that $\epsilon = 0{\cdot}8$ is the lower limit that precludes solid solubility of an additive within a host system. For CI Disperse Orange 44 (Fig 1a) and CI Disperse Red 54 (Fig. 1b), $\epsilon = 0{\cdot}91$. This is a quick useful guide, but a more detailed understanding of the likely effects of a guest impurity can only be obtained through examination of the crystal packing.

3.3.2 High resolution powder diffraction

High resolution X-ray diffraction patterns taken on the SRS showed no significant changes occur in the unit cell dimensions on incorporation of the guest impurity molecule. This is also shown in Fig. 6a and b, where the major peaks occur at the same position in the pure and mixed crystal samples. The mixed crystal sample is obviously less crystalline, though the pattern is essentially the same. Table 6 contains the 2θ values for four different reflections representing the three orthogonal directions in the unit cell. The values listed include calculated ones based on the crystal structure unit cell and those indexed from the high resolution patterns for pure and mixed crystal samples.

TABLE 6
Calculated and Experimental Peak Positions (2θ values)

Reflection	*Calculated*	*Pure*	*Mixed crystal*
(100)	4·32	4·36	4·32
(200)	8·64	8·68	8·62
(002)	12·45	12·48	12·44
(012)	14·00	14·04	14·01

It would appear that there is a small, but constant (in both size and sense), mismatch between the pure and mixed crystal diffraction traces. Such small differences indicate very little change in the unit cell dimensions. The offset could be due to slightly different zero-point error for each of the samples, which results from slightly different sample heights in each sample.

In order to determine whether the pattern broadening for the pure and mixed crystal samples was due to changes in crystallite size or strain within the crystallites, the data were further analysed. The (0*kk*) reflections are weak and this hindered an analysis of the bc diagonal. The strength of the (100) and (200) reflections enables a comparison of the (*h*00) direction between the two samples.

For both datasets a plot of $\beta\cos\theta$ against $\sin\theta$ (where β is the refined peak width in degrees 2θ) for the (100) and (200) reflections yields a straight line whose intercept gives a measure of the crystallite size, and whose slope gives a measure of the crystallite strain in the reciprocal lattice direction. This approach is often referred to as the Williamson–Hall method.[26]

In terms of crystallite size, the analysis suggests that the crystals in the pure sample are larger by approximately a factor of two than the mixed crystal sample. The mixed crystal sample is also five times more strained along this *h*00 direction than the pure sample.

3.3.3 Crystal packing calculations

CERIUS was used to examine the effect of the impurity incorporation on the crystal lattice. The CI Disperse Red 54 molecule was constructed from a CI Disperse Orange 44 molecule with the additional $-COOCH_3$ added on using standard bond lengths and angles. The charges over the guest impurity molecule were recalculated.

The similarity of the host and guest molecules allowed the guest molecule to be fitted onto and replace a host molecule within the lattice, the only difference being in the flexible end groups, where the larger $-COOCH_3$ group in the guest was replacing a cyano group in the host structure. The modelling suggests that the $-COOCH_3$ group is most likely to cause disruption

TABLE 7
Calculated Lattice Energies for Pure and Mixed Crystal CI Disperse Orange 44

System	*Dopant concentration (%)*	*Lattice energy (kcal mol^{-1})*
Pure CI Disperse Orange 44	0·0	–32·3
Case 1	12·5	–27·3
Case 2	50·0	–12·3

along the *a*-direction and this is consistent with the strain results observed from the high resolution XRD patterns.

Two different cases were considered. In Case 1, one host molecule in the unit cell was replaced with one guest molecule, giving an overall concentration of 12·5%. In Case 2, one of the two independent molecules in the asymmetric unit was replaced, giving an overall concentration of 50%. The lattice energy was then minimised for each of these cases.

During minimisation, the unit cell dimensions and space group symmetry were kept constant, as the X-ray diffraction patterns indicate that the guest is incorporated without major changes in the host structure. During minimisation all the molecules were allowed to rotate around the three crystal axes and to translate in three directions. In addition, the guest molecule leg containing the $-COOCH_3$ impurity was allowed freedom to rotate around all torsion angles within the leg in order that it find its optimum arrangement within the lattice. The legs containing the $-CH_2CH_2CN$ units were not allowed to rotate. The calculated lattice energies are given in Table 7.

These initial modelling studies seem to indicate that the lattice energy drops by about 5 kcal mol^{-1} for each 10% of guest included. In experimental studies, 10% guest results in the melting point falling by 13°C and the heat of fusion dropping by about 2·1 kcal mol^{-1}.

The bulkier $COOCH_3$ group might be expected to cause more disruption and upset the lattice structure to an extent where it should alter the lattice

TABLE 8
Short Intermolecular Contacts Between Dopant and Host Structure in Case 1

Intermolecular contact		*Distance (Å)*
Dopant	*Host*	
C=O	CN	3·1
–O–	CN	3·0
C=O	H–C	2·5
C–H	O=N	2·6

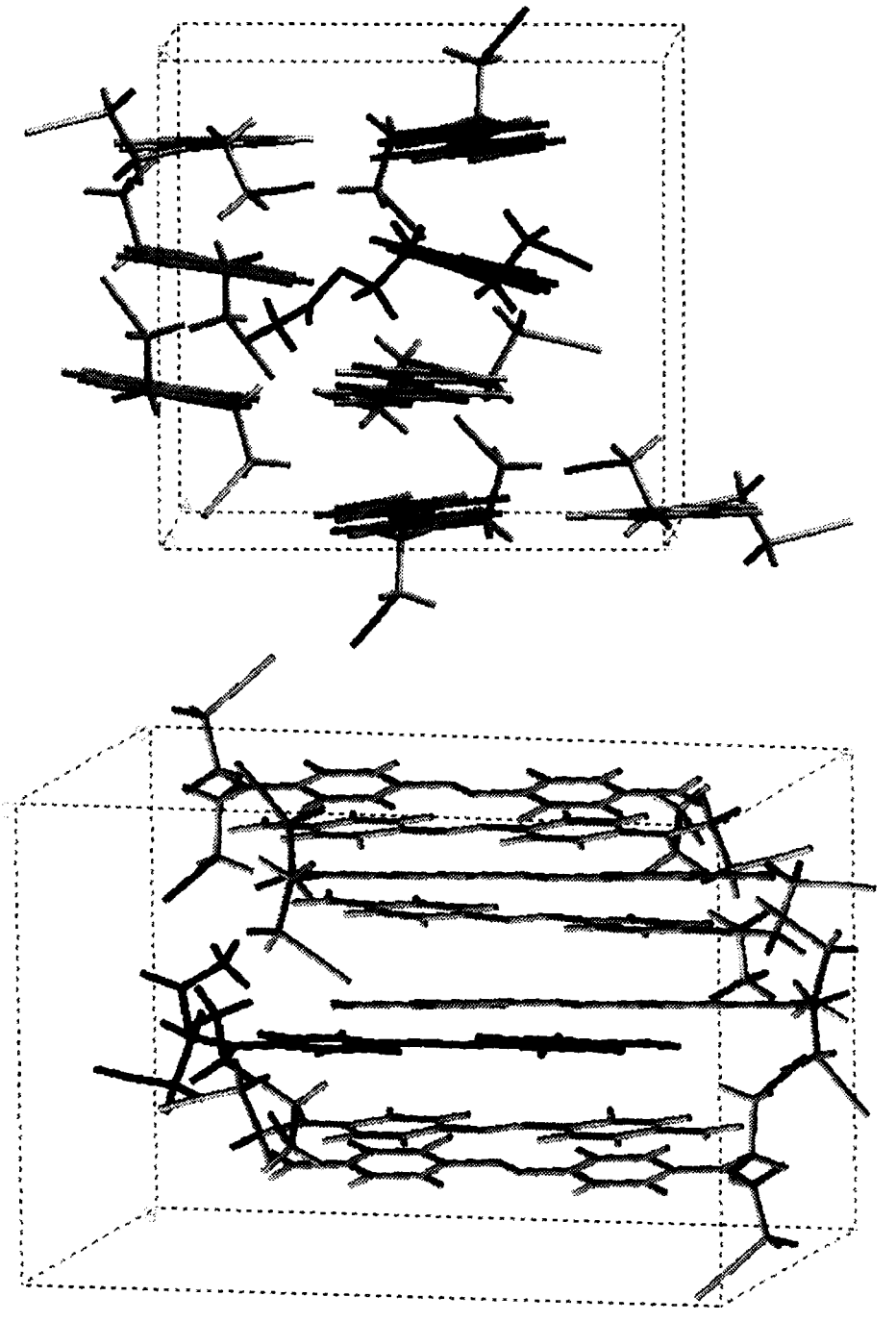

Fig. 9. The doped mixed crystal cell showing one CI Disperse Red 54 molecule in the unit cell. The CI Disperse Red 54 molecule is darker. The structure results from case study 1. The top view is down the *a*-axis, the bottom view up the *b*-axis.

parameters. However its bulky nature (compared to a cyano group) and overall disruption of the host structure seems to be compensated for (partially at least) by the formation of interactions from the $COOCH_3$ to the cyano and nitro groups of the surrounding host molecules. A summary of some of these contacts determined from the minimised Case 1 study is given in Table 8. The unit cell for this structure is given in Fig. 9.

4 CONCLUSIONS

The crystal structure of CI Disperse Orange 44 consists of columns containing molecules held together with π–π interactions. These columns consist of alternating dimer arrangements 3·3 and 3·4 Å apart. The columns are held together through Cl----H non-bonded interactions in one direction and a network of electrostatic interactions involving the cyano groups in the crystallographic *a*-direction. The structural arrangement is similar to that found for other donor–acceptor azobenzenes.

Crystal packing calculations reproduce the important intermolecular interactions within the system well, with the calculated lattice energies being within 2 kcal mol^{-1} of the experimental value.

A guest impurity molecule CI Disperse Red 54 can be incorporated into the lattice of CI Disperse Orange 44 with very little change in the basic unit cell dimensions. The incorporation of up to 10% of the dopant reduces the melting point by 13°C and reduces the heat of fusion by about 2·1 kcal mol^{-1}. Simple lattice energy calculations in the presence of this impurity imply a drop in the lattice energy of 5 kcal mol^{-1} might be expected.

The initial modelling suggests that the guest molecule would disrupt along the *a*-direction and this is consistent with the results of lattice strain analysis carried out using the high resolution X-ray diffraction traces.

ACKNOWLEDGEMENTS

Mr M. Edmondson for the provision of the standard diffractograms, Dr J. I. MacNab for the sublimation enthalpy measurements and Mr D. Brierley, Dr D. J. Edwards and Mr L. A. Mather for discussions on the properties of disperse dyes.

REFERENCES

1. Langhals, H., Demmig, S. T. & Potrawa, T. H., *J. Pract. Chem.* **333** (1991) 733.

2. Iqbal, A., Jost, M., Kirchmayr, R., Pfenninger, J., Rochat, A. & Wallguist, Q., *Bull. Soc. Chim. Belg.*, **97** (1988) 615.
3. Hadicke, E. & Grazer, F., *Acta Cryst.*, **C42** (1986) 189.
4. Whitaker, A. & Walker, N. P. C., *Acta Cryst.*, **C43** (1987) 2137.
5. Whitaker, A., *Acta Cryst.*, **C44** (1988) 1587.
6. Biedermann, W., *J. Soc. Dyers Colour.*, **87** (1971) 105.
7. Shimizu, T., Ohkubo, S. Kimura, M. Tabata, I. & Hori, T., *J. Soc. Dyers Colour.*, **10** (1987) 132.
8. Nishida, K., Ishihara, E., Osaka, T., & Koukitu, M., *J. Soc. Dyers Colour.*, Feb (1977) 52.
9. Karpov, V. V., Rodionova, G. N. Krutovskaya, I. V., Gandel'sman, L. Z., Khomenko, L. A. & Yagupolskii, L. M., *Dyes and Pigments*, **5** (1984) 285.
10. Maginn, S. J., Bullock, J. F. & Docherty, R., *Dyes and Pigments*, **23** (1993) 159.
11. Sheldrick, G. M., *SHELXS86*, Program for Crystal Structure Determination, University of Gottingen, 1986.
12. Sheldrick, G. M., *SHELXL93*, Program for Crystal Structure Refinement, University of Gottingen, 1993.
13. Harris, D. M., Tremayne, M., Lightfoot, P. & Bruce, P. G., *J. Am.. Chem. Soc.*, **116** (1994) 3543.
14. Fagan, P. G., Roberts, K. J., Potts, G. D., Jones, W., Docherty, R. & Chorlton, A. P., *J. Materials Chem.* (submitted).
15. Freeman, H. S., Posey, J. C. & Singh, P., *Dyes and Pigments*, **20** (1992) 279.
16. Charlton, M. H., Docherty, R., McGeein, D. J. & Morley, J. O., *J. Chem. Soc., Faraday Trans.*, **89** (1993) 1671.
17. Allen, F. H., Kennard, O., Watson, D. G., Brammer, L., Orpen, A. G. & Taylor, R., *J. Chem. Soc., Perkin Trans. II* (1987) S1.
18. Desiraju, G. M., *Crystal Engineering: The Design Of Organic Solids*. Elsevier, Amsterdam (1989).
19. Maginn, S. J., Compton, R. G., Harding, M. S., Brennan, C. M. & Docherty, R., *Tetrahedron Lett.*, **34** (1993) 4349.
20. PCK83. A Program For Molecular Crystal Packing Analysis. D. E Williams, Quantum Chemistry Program Exchange Program No. 481.
21. CERIUS (V.3.0) Molecular Simulations Inc. 240/250 The Quorum, Barnwell Road, Cambridge, England.
22. Bernstein, J. & Hagler, A. T., *J. Am. Chem. Soc.*, **100** (1978) 6.
23. MOPAC (Version 6.0) Quantum Chemistry Exchange Program No. 455.
24. Rappe, A. K. & Goddard, W. A., *J. Phys. Chem.*, **95** (1991) 3358.
25. Kitaigorodskii, A. I., *Mixed Crystals*. Springer, New York (1984).
26. Williamson, G. K. & Hall, W. H., *Acta Metall.*, **1** (1953) 22.